Regional differences in the three-dimensional bone microstructure of the radial head

Viveen, Jetske; Perilli, Egon; Jaarsma, Ruurd L.; Doornberg, Job N.; Eygengaal, Denise; Bain, Gregory I.

Published in:
Archives of orthopaedic and trauma surgery

DOI:
10.1007/s00402-020-03665-3

Publication date:
2022

Archives of Orthopaedic and Trauma Surgery (2022) 142:165–174
https://doi.org/10.1007/s00402-020-03665-3

TRAUMA SURGERY

Regional differences in the three-dimensional bone microstructure of the radial head: implications for observed fracture patterns

Jetske Viveen[1,2] · Egon Perilli[3] · Ruurd L. Jaarsma[1] · Job N. Doornberg[1,2,4] · Denise Eygengaal[2,5] · Gregory I. Bain[1]

Received: 23 February 2020 / Accepted: 15 October 2020 / Published online: 10 November 2020

Abstract

Introduction A characterization of the internal bone microstructure of the radial head could provide a better understanding of commonly occurring fracture patterns frequently involving the (antero)lateral quadrant, for which a clear explanation is still lacking. The aim of this study is to describe the radial head bone microstructure using micro-computed tomography (micro-CT) and to relate it to gross morphology, function and possible fracture patterns.

Materials and methods Dry cadaveric human radii were scanned by micro-CT (17 µm/pixel, isotropic). The trabecular bone microstructure was quantified on axial image stacks in four quadrants: the anterolateral (AL), posterolateral (PL), posteromedial (PM) and anteromedial (AM) quadrant.

Results The AL and PL quadrants displayed the significantly lowest bone volume fraction and trabecular number (BV/TV range 12.3–25.1%, Tb.N range 0.73–1.16 mm^{-1}) and highest trabecular separation (Tb.Sp range 0.59–0.82 mm), compared to the PM and AM quadrants (BV/TV range 19.9–36.9%, Tb.N range 0.96–1.61 mm^{-1}, Tb.Sp range 0.45–0.74 mm) ($p = 0.03$).

Conclusions Our microstructural results suggest that the lateral side is the "weaker side", exhibiting lower bone volume faction, less trabeculae and higher trabecular separation, compared to the medial side. As the forearm is pronated during most falls, the underlying bone microstructure could explain commonly observed fracture patterns of the radial head, particularly more often involving the AL quadrant. If screw fixation in radial head fractures is considered, surgeons should take advantage of the "stronger" bone microstructure of the medial side of the radial head, should the fracture line allow this.

Keywords Elbow · Radial head · Fracture · Micro-CT · Trabeculae

Introduction

Although many anatomical and imaging studies on the gross anatomy of the proximal radius have been published [1–6], only two studies used high-resolution three-dimensional (3D) imaging methods such as micro-computed tomography (micro-CT) [7, 8]. In these studies, the age-related changes in the bone microstructure were visualized [8] and the unique anatomical variance of the four quadrants within the radial head examined [7]. However, to the best of our knowledge, the 3D microstructure of the trabecular bone within the radial head has not yet been described using micro-CT in relation to clinically-relevant fracture patterns.

Micro-CT allows examination of bone segments without coring at spatial resolutions in the 10–20 µm range, enabling the quantification of bone microstructure [9–12]. Previous studies using this imaging modality enhanced clinical practice [9, 13], whereas studying the greater tuberosity of the proximal humerus improved the surgical approach of trans-osseous equivalent rotator cuff repair for instance [14]. From a biomechanical point of view, it aids understanding the distribution of the bone microstructure and put it in relation with possible loads within the bone, leading to possible fractures [15].

✉ Jetske Viveen
jetskeviveen@gmail.com

1 Department of Orthopedic and Trauma Surgery, College of Medicine and Public Health Flinders University and Flinders Medical Centre, Adelaide, SA 5042, Australia

2 Department of Orthopedic Surgery, Amsterdam University Medical Centers, Amsterdam, The Netherlands

3 Medical Device Research Institute, College of Science and Engineering, Flinders University, Tonsley, SA 5042, Australia

4 Groningen University, Groningen University Medical Centre, Groningen, The Netherlands

5 Upper Limb Unit, Department of Orthopedic Surgery, Amphia Hospital, Breda, The Netherlands

Fractures of the radial head are relatively common and comprise approximately four percent of all fractures in the human body [16]. Radial head fractures could have possible elbow instability as result, since the radial head is an important secondary stabilizer of the elbow joint [17, 18]. The anterolateral quadrant of the radial head has been found most frequently involved in radial head fractures (Figs. 1, 2) [5, 19, 20]. Several hypotheses about the influence of the trauma mechanism [21] and gross bone anatomy on this fracture phenomenon are available, however, a clear explanation is still lacking [4, 6, 7, 21, 22]. An improved characterization of the internal trabecular bone microstructure of the radial head could therefore provide a better understanding of these possible fracture patterns.

The aim of this study is to describe the bone microstructure of the radial head using micro-CT and relate it to gross morphology and function. This study will contribute to our understanding of the bone microstructure in relation to possible mechanical loads and fractures occurring within the four quadrants of the radial head. This could ultimately aid in enhancing fracture treatment in daily practice. We hypothesize that possible regional differences in the trabecular microstructure of the radial head (mechanical "weak spots"), in combination with the trauma mechanism [21], could explain commonly observed fracture patterns.

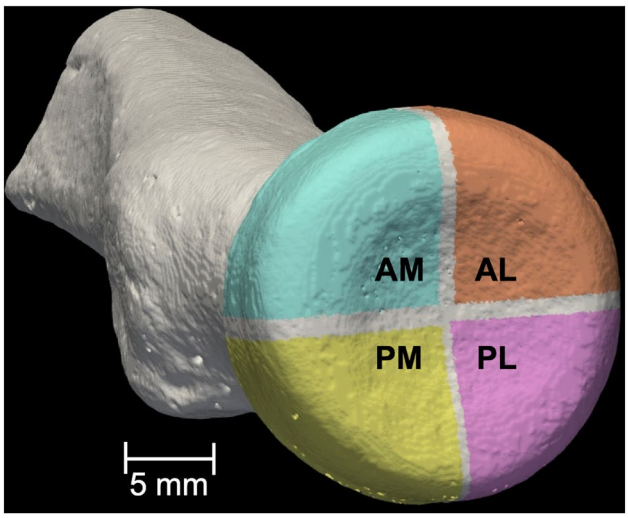

Fig. 1 3D micro-CT rendering of a right proximal radius, showing the 4 quadrants of the radial head. *AL* anterolateral, *PL* posterolateral, *PM* posteromedial, *AM* anteromedial

Materials and methods

Specimens

Six intact cadaveric dry radii (three left, three right) were collected from Ray Last Laboratories (The University of Adelaide, Adelaide, SA, Australia). The committee of the Ray Last Laboratories approved this study. Since no donor characteristics were available, approval by the human ethics research committee was not required.

Micro-CT scanning

A micro-CT system (SkyScan model 1076, Skyscan-Bruker, Kontich, Belgium) was used to scan the specimens in air. Scans were performed with a source voltage of 80 kVp, current of 120 µA, rotation step of 0.6° over 180° rotation, 1 frame averaging and a 0.5-mm thick aluminum filter for beam hardening reduction. The isotropic resolution was 17 µm per pixel [9]. For each specimen, cross-section images of the entire proximal radius (up to 74 mm long, 21 mm wide) were reconstructed. Stacks of axial, sagittal and coronal slices were created (software Dataviewer, Skyscan-Bruker). CT Analyser (v1.14.4.1, Skyscan-Bruker) and ParaView open source software (available at www.paraview.org/, Kitware Inc.) were used for analyses.

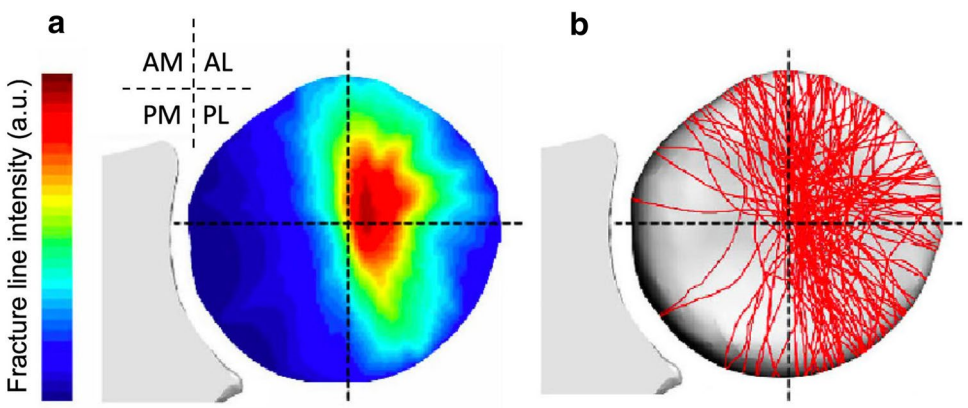

Fig. 2 Heat (**a**) and fracture (**b**) map illustrating fracture line distribution of the radial head as described by Mellema et al. [5] (reprinted from Mellema et al. © 2016, with permission from Elsevier)

Microstructural analysis

To reproduce reliable axial, sagittal and coronal image stacks in all specimen, the images were rotated in 3D (software Dataviewer) so that the medial and lateral tip of the radial head were positioned on a horizontal line in the sagittal and coronal view. In addition, in these images, the most prominent point of the radial tuberosity was rotated 132° clockwise (left specimens) or counter clockwise (right specimens) (Dataviewer), to simulate a neutral position of the forearm as reported by van Leeuwen et al. [20]. Both qualitative and quantitative assessments were performed on the micro-CT image stacks. Qualitative assessments included visually observed trabecular patterns in the entire proximal radius. Quantitative assessments included calculation of the trabecular microstructure in the four quadrants of the radial head as explained below.

The trabecular bone microstructure was quantified by performing histomorphometry analysis (CT Analyser) in cylindrical volumes of interest (VOI) selected via software as follows. The radial head was first divided in 4 quadrants (Fig. 1) and each quadrant was subdivided into 3 equiangular sectors, each inscribing an angle of 30° (Fig. 3a). The cylindrical VOIs were centered on the midline of each sector and placed as close as possible to the anterior, posterior, medial or lateral cortex of the radial head, containing only trabecular bone. The VOIs were selected on the axial image stack (green horizontal line, Fig. 3a inset and Fig. 3b), 3 mm distal from the most proximal axial image stack where the 12 cylindrical VOIs were fitting, without involving the cortex of the proximal side (blue horizontal line, Fig. 3a inset and Fig. 3b). The VOIs had a diameter of 3.5 mm and height of 3 mm (to satisfy the continuum condition for trabecular bone analysis) [9, 13, 23]. Analyses were performed in the following four regions (quadrants) (Figs. 1, 3a): the anterolateral (AL), posterolateral (PL), posteromedial (PM) and anteromedial (AM) quadrant (orange, pink, yellow and blue circles, respectively). Then, for each quadrant, the average of the values of the VOIs of the 3 sectors was taken.

For the trabecular microstructure analysis, images were binarized separating bone from non-bone using uniform thresholding in all specimens [11, 12]. The analysis included bone volume fraction (BV/TV in %; calculated as the voxels segmented as bone within the VOI, divided by the voxels constituting the examined VOI), trabecular thickness (Tb.Th. in mm; 3D measure of the average thickness of the trabeculae [24]), trabecular number (Tb.N in mm^{-1}; the number of trabecular plates per unit length [25]), trabecular separation (Tb.Sp in mm; 3D measure of the mean distance between the trabeculae [26]) and structure model index (SMI) which describes the ratio of rod- to plate-like trabecular structures, ranging in value from 0 (ideal plate-like structure) to 3 (ideal rod-like structure), with intermediate values indicating a mixed structure [13, 26, 27].

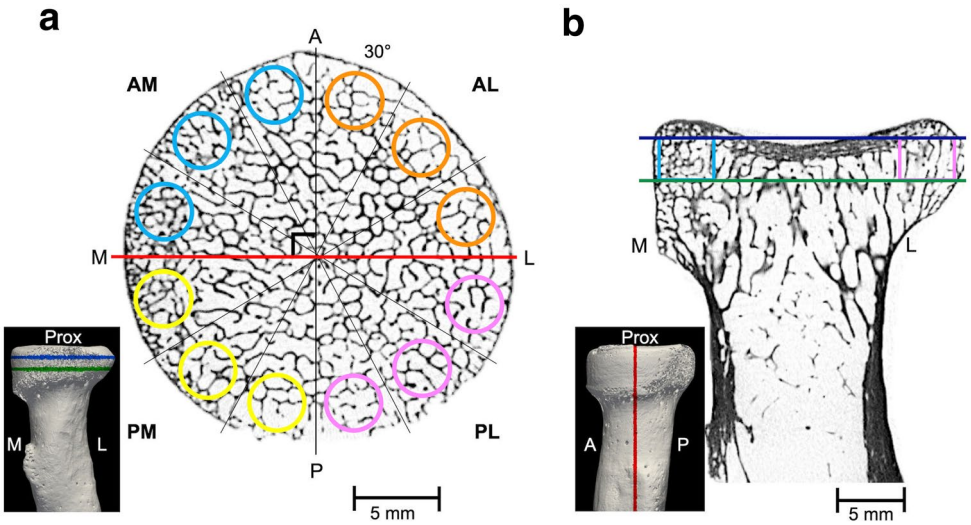

Fig. 3 Proximal radius, micro-CT images: axial (**a**) and sagittal (**b**) view. **a** Micro-CT cross-section, axial view of "bottom plane" (green line in inset), regions for quantitative 3D trabecular microstructure analysis (three cylindrical volumes of interest, 3.5 mm diameter and 3 mm height, indicated by circles, per quadrant): anterolateral quadrant (AL, orange circles), posterolateral quadrant (PL, pink circles), posteromedial quadrant (PM, yellow circles) and anteromedial quadrant (AM, blue circles). Red line shows location of sagittal plane in **b**. **b** Micro-CT cross-section, sagittal view, the locations of the cylindrical volumes of interest are indicated by the blue and pink rectangles. Dark blue and green horizontal line show position of "top" and "bottom" axial plane, respectively. Inset in **a** and **b**: 3D micro-CT rendering of the proximal radius, showing the location of the "top" (dark blue line) and "bottom" (green line) axial plane and sagittal plane (red line) used for reference. *M* medial, *L* lateral, *A* anterior, *P* posterior, *Prox* proximal

Statistical analysis

StatView (SAS Institute Inc., Version 5.0.1) was used for statistical analysis. To compare measurements among the four quadrants, a non-parametric Friedman test was used, which, if significant, was followed by a post-hoc Wilcoxon signed rank test. Statistical significance was set at $p < 0.05$.

Results

Qualitative assessment of trabecular patterns

On the sagittal cross-section image stack (3D rendering, 1.5 mm thick), main trabecular patterns were identified in the proximal radius (Fig. 4a). Groups of trabecular struts were observed spanning from the foveal joint surface towards the medial and lateral cortices (dashed blue lines, Fig. 4b). On the lateral side of the radial head, the trabeculae are spanning mainly orthogonal to the joint surface, whereas on the medial side of the radial head, trabeculae appear more multidirectional and include the orthogonal struts spanning from the fovea.

Quantitative assessment of trabecular microstructure

The trabecular bone histomorphometry results showed significant differences among the regions analyzed (see Fig. 5 and Table 1 for average values). The trabecular bone volume fraction and number were significantly lower in the AL and PL quadrants (BV/TV range 12.3–25.1%, Tb.N range 0.73–1.16 mm^{-1}) compared to the PM and AM quadrants (BV/TV range 19.9–36.9%, Tb.N range 0.96–1.61 mm^{-1}) ($p = 0.03$). Correspondingly, the trabecular separation within the AL and PL quadrants (range 0.59–0.82 mm) was significantly higher compared to the AM and PM quadrants (range 0.45–0.74 mm) ($p = 0.03$). The PL quadrant had a lower trabecular thickness (range 0.16–0.24 mm) and higher SMI (range 1.11–1.70) compared to the PM and AM quadrants (Tb.Th range 0.17–0.29 mm, SMI range 0.74–1.50) ($p = 0.03$).

In Fig. 6 and Table 2, a comparison is made between a specimen showing an overall high bone volume fraction (Fig. 6a–c, radius#1, BV/TV = 30.4%, range 21.7–42.1%) and low bone volume fraction (Fig. 6d–f, radius#2, BV/TV = 20.9%, range 14.3–31.4%). For each specimen, the "overall" value was calculated as the average of the 12 cylindrical VOIs. Regardless of the overall bone volume fraction of the specimens, the lateral side showed less and thinner trabeculae, resulting in a lower bone volume fraction and higher trabecular separation compared to the medial side, in both specimens (Fig. 6c vs. f, Table 2). Consistently, when calculating the ratio "BV/TV lateral / BV/TV medial", the ratio was below unity and it was 0.67 on average when considering all the 6 specimens together, whereas it was 0.68 for the overall high BV/TV and 0.76 for the overall low BV/TV specimen, respectively.

Discussion

In this study we reported on the 3D microstructure of the trabecular bone within the radial head. High resolution micro-CT imaging was used to perform both qualitative and quantitative assessments. Consistently among the radii examined, the lateral side showed a lower bone volume faction, less

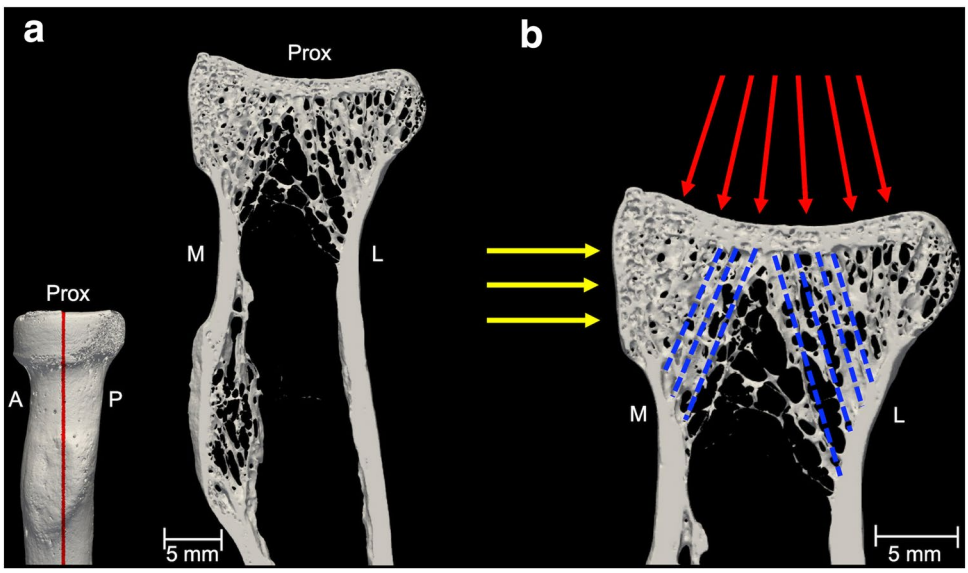

Fig. 4 3D-rendering of sagittal micro-CT cross-section image stacks (1.5-mm thick volume) of the proximal radius. **a** Sagittal 3D micro-CT rendering. **b** Possible loads on the radial head: line of action of the humerus (red arrows) and of the proximal ulna (yellow arrows). Dashed blue lines: trabeculae spanning from the joint surface to the medial and lateral cortex. Inset, bottom left corner: 3D micro-CT rendering of the proximal radius, showing the location (red line) of the image. *A* anterior, *P* posterior, *M* medial, *L* lateral, *Prox* proximal

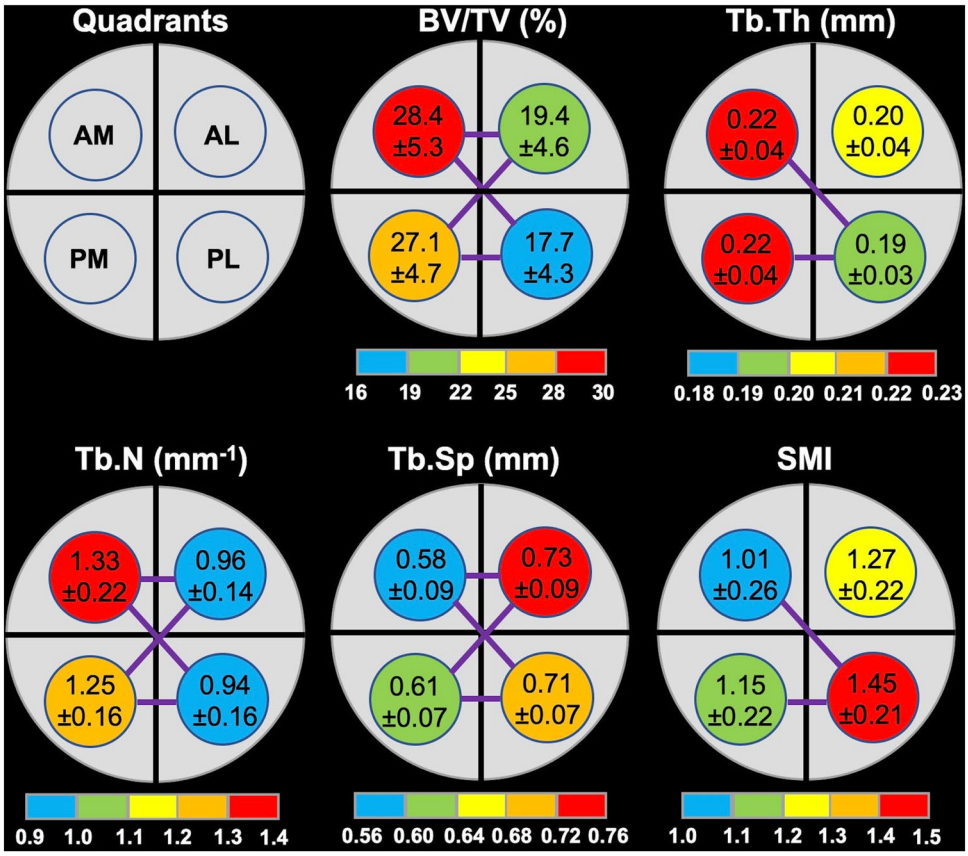

Fig. 5 Trabecular bone microstructure (mean ± standard deviation, 6 radii) quantified from micro-CT image stacks in the 4 quadrants (average of 3 cylinders per quadrant, each 3.5 mm in diameter and 3 mm in height) in the locations as described in Fig. 3a. Purple lines connecting the quadrants indicate statistically significant differences among these quadrants: The AL and PL quadrants exhibit statistically significant differences in BV/TV, Tb.N and Tb.Sp when compared to the PM and AM quadrants ($p < 0.05$). The PL quadrant exhibit statistically significant differences in Tb.Th and SMI when compared to the PM and AM quadrants ($p < 0.05$)

Table 1 Trabecular bone microstructure (mean ± standard deviation, 6 radii) measured in the 4 quadrants (average of 3 cylinders per quadrant, each cylinder 3.5 mm in diameter and 3 mm in height) in the locations as described in Fig. 3a

	AL	PL	PM	AM
BV/TV (%) [min, max]	19.4 ± 4.6* [12.9, 24.3]	17.7 ± 4.3* [12.3, 25.1]	27.1 ± 4.7 [19.9, 35.5]	28.4 ± 5.3 [20.4, 36.9]
Tb.Th (mm) [min, max]	0.20 ± 0.04 [0.15, 0.27]	0.19 ± 0.03^ [0.16, 0.24]	0.22 ± 0.04 [0.18, 0.29]	0.22 ± 0.04 [0.17, 0.27]
Tb.N (mm^{-1}) [min, max]	0.96 ± 0.14* [0.74, 1.14]	0.94 ± 0.16* [0.73, 1.16]	1.25 ± 0.16 [0.95, 1.37]	1.33 ± 0.22 [1.03, 1.61]
Tb.Sp (mm) [min, max]	0.73 ± 0.09* [0.61, 0.82]	0.71 ± 0.07* [0.59, 0.79]	0.61 ± 0.07 [0.56, 0.74]	0.58 ± 0.09 [0.45, 0.68]
SMI [min, max]	1.27 ± 0.22 [1.04, 1.60]	1.45 ± 0.21^ [1.11, 1.70]	1.15 ± 0.22 [0.90, 1.50]	1.01 ± 0.26 [0.74, 1.47]

AL anterolateral, *PL* posterolateral, *PM* posteromedial, *AM* anteromedial quadrants

*The AL and PL quadrants exhibit statistically significant differences in BV/TV, Tb.N and Tb.Sp when compared to the PM and AM quadrants ($p < 0.05$)

^The PL quadrant exhibit statistically significant differences in Tb.Th and SMI when compared to the PM and AM quadrants ($p < 0.05$)

trabeculae and higher separation, compared to the medial side.

This study has several limitations. Firstly, the sample size of 6 cadaveric specimens was small. However, to account for this, we used non-parametric statistics (Friedman test, followed by Wilcoxon signed rank test) in the comparisons. Moreover, no donor characteristics were available. Therefore, it was not possible to make any grouping based on age, gender or lifestyle. Despite these limitations, statistically significant differences were observed among the quadrants examined.

As bone adapts to the daily mechanical loads it is subjected to (Wolff's law) [28], the investigation of its microstructure may reflect the distribution of these everyday loads

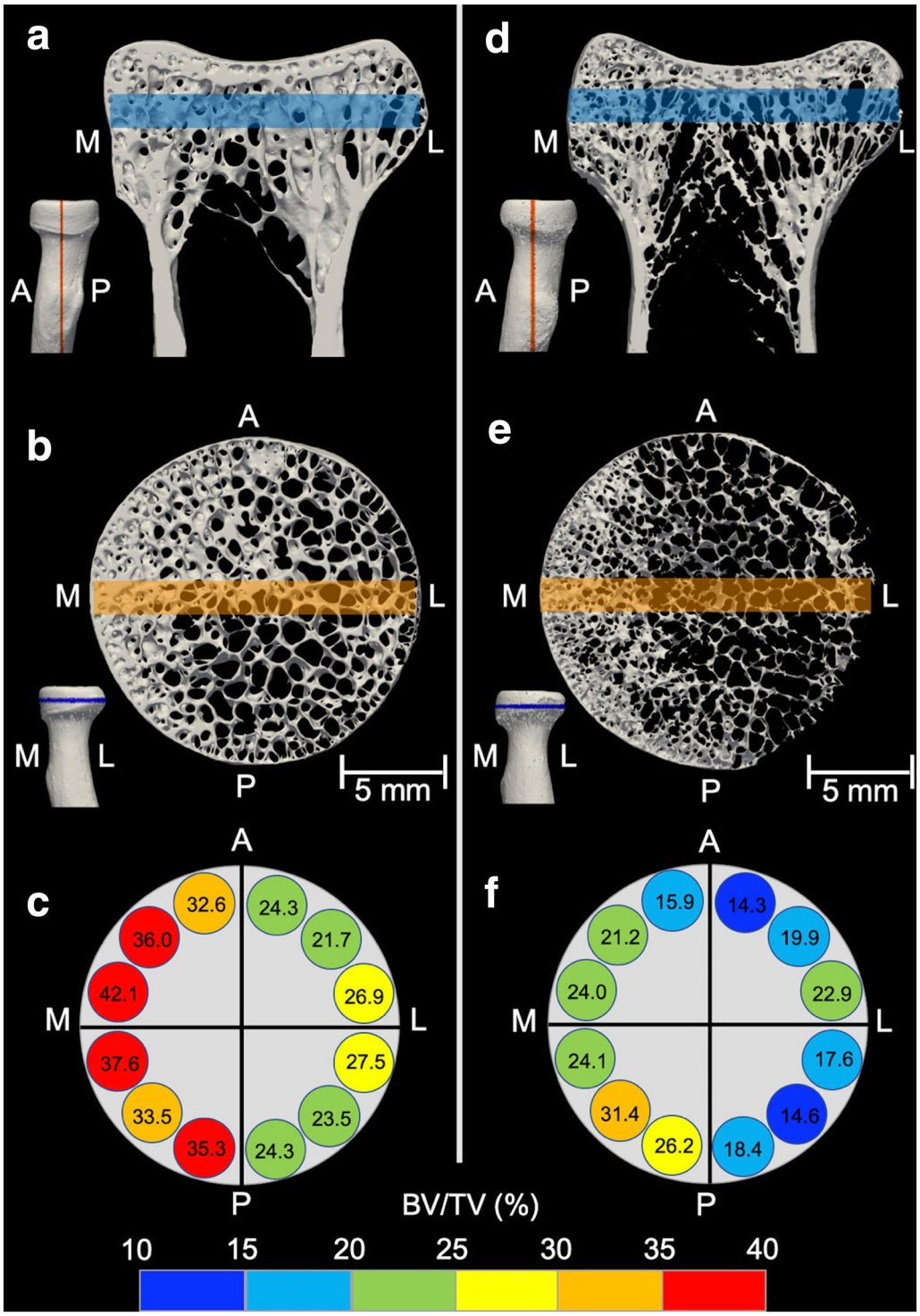

Fig. 6 3D-rendering of sagittal (**a**, **d**) and axial (**b**, **e**) micro-CT cross-section image stacks (1.5 mm-thick volume) of two proximal radii, exhibiting overall high bone volume fraction (BV/TV = 30.4%, left #1) and low bone volume fraction (BV/TV = 20.9%, right #2), measured as average of the 12 VOI's as described in Fig. 3a. Bone microstructure comparison: despite the difference in overall bone volume fraction between the two specimens, the medial side showed the highest bone volume fraction compared to the lateral side (**c**, **f**). See Table 2 for detailed trabecular bone values in each region. Insets left and right: 3D micro-CT rendering of the proximal radius, showing the location of the sagittal plane (orange line) and axial plane (blue line) used for reference. *M* medial, *L* and lateral, *A* anterior, *P* posterior

Table 2 Trabecular bone microstructure values (mean ± standard deviation) of two proximal radii showing overall high bone volume fraction (BV/TV = 30.4%, #1) and low bone volume fraction (BV/TV = 20.9%, #2; Fig. 6) measured in the 4 quadrants (average of 3 cylinders per quadrant, each cylinder 3.5 mm in diameter and 3 mm in height) in the locations as described in Fig. 3a

		AL	PL	PM	AM
BV/TV (%)	Radius #1 (high)	24.3 ± 2.6	25.1 ± 2.1	35.5 ± 2.1	36.9 ± 4.8
	Radius #2 (low)	19.1 ± 4.4	16.9 ± 2.0	27.2 ± 3.8	20.3 ± 4.2
Tb.Th (mm)	Radius #1 (high)	0.23 ± 0.01	0.24 ± 0.02	0.29 ± 0.04	0.27 ± 0.02
	Radius #2 (low)	0.20 ± 0.02	0.20 ± 0.02	0.21 ± 0.02	0.20 ± 0.01
Tb.N (mm^{-1})	Radius #1 (high)	1.04 ± 0.07	1.07 ± 0.05	1.23 ± 0.17	1.36 ± 0.14
	Radius #2 (low)	0.96 ± 0.15	0.89 ± 0.09	1.27 ± 0.06	1.03 ± 0.14
Tb.Sp (mm)	Radius #1 (high)	0.74 ± 0.04	0.69 ± 0.01	0.62 ± 0.02	0.57 ± 0.05
	Radius #2 (low)	0.81 ± 0.11	0.76 ± 0.04	0.56 ± 0.03	0.68 ± 0.09
SMI	Radius #1 (high)	1.04 ± 0.08	1.11 ± 0.09	0.90 ± 0.29	0.74 ± 0.22
	Radius #2 (low)	1.26 ± 0.14	1.50 ± 0.06	1.30 ± 0.14	1.47 ± 0.12

and aid understanding them, because the alignment of the elbow moves from varus to valgus as the elbow goes from flexion to extension, and most daily activities are performed with a flexed elbow and pronated forearm [29]. Within the lateral side of the radial head, the trabeculae span almost orthogonal (blue lines) to the foveal joint surface (Fig. 4b). The lateral side, which includes the "safe zone", never articulates with the proximal ulna [19], is mainly subjected to compressive axial loads (red arrows, Fig. 4b) coming through the foveal joint surface from the humerus during the many everyday activities which involve elbow flexion [29–31]; this is consistent with the aforementioned orthogonal trabecular bone pattern found in this part of the radial head, which may enable the load to be transferred towards the radial cortex. In contrary, more multidirectional trabeculae are observed on the medial side of the radial head (Fig. 4a); this multidirectionality of the microstructure is consistent with the medial side being subjected to a combination of shear loads coming from the proximal ulna (yellow arrows, Fig. 4b) during daily activities involving pronation and supination [29–31], as well as the compressive axial loads through the foveal joint surface coming from the humerus (red arrows, Fig. 4b).

Radial head fractures are most commonly caused by a fall on an outstretched hand and usually occur as a result of a low energy fall in females above 50 years suffering from osteoporosis or in younger males as a result of a high energy trauma [32, 33]. In these fractures, the AL quadrant is found most frequently involved as revealed in fracture mapping studies (Fig. 2) [5, 20]. This could be at least in part explained by the trauma mechanism, since the forearm is pronated during most falls, resulting in the AL quadrant rotating to fully anterior and receiving an "unusually high" compressive load from the humerus mostly in that quadrant [21]. Additionally, the present results show that the lateral region of the radial head has significantly lower amount of bone compared to medially, probably due to the habitual (less) loading it is subjected to. In case of an axial impact during a fall with an abnormally high compressive load on the joint surface, the radial head is more likely to fail in the lateral part as this is potentially weaker than medially at the microstructural level [34]. Therefore, this suggests that the underlying bone microstructure might be important in explaining these possible fracture patterns; in fact, independently of the overall amount of bone of the examined specimen (whether a specimen had a generally low or high bone volume fraction, which, potentially could represent an elderly or young subject, respectively), the lateral side presents less bone than medially (Fig. 6c, f) and could therefore also act as the weaker region in case of a fall (weakest link) [34]. Hence, the trabecular microstructure, in combination with the nature of the trauma mechanism, could explain the possible fracture patterns of the radial head, in particular more often involving the lateral quadrants.

Two previous studies performed imaging of the radial head using micro-CT [7, 8]. Adikrishna et al. describes the proximal corner of the PM quadrant as beveled [7], with the "rim" exhibiting higher subchondral bone thickness (apparently including also the cortical bone in their thickness measurement) in the PM quadrant compared to the other quadrants, which in principle is aligned with the present results. However, that study did not specifically investigate the trabecular bone microarchitecture and did not quantify it in terms of histomorphometric parameters. Gebauer et al. visualized the age-related changes in bone microarchitecture of the radial head [8]. Through histology, significantly lower trabecular bone volume per tissue volume and trabecular thickness in advanced age was found, with changes in females being more pronounced compared to males, probably also due to increased bone turnover in aging women particularly after menopause [35]. However, that study did not quantify and compare the trabecular bone among different subregions (quadrants). Whereas previous studies might contribute to explain the occurrence of radial head fractures and particularly in females > 50 years [32], no study has yet quantified local differences in trabecular bone

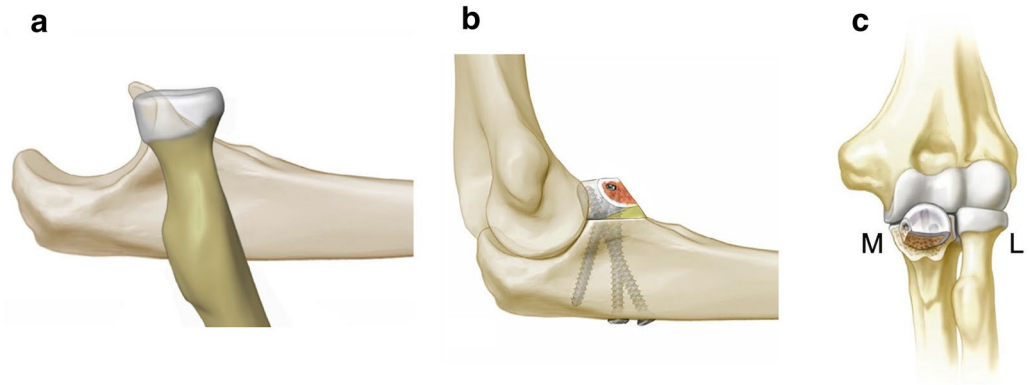

Fig. 7 The use of the medial side of the radial head as an autograft for the fractured coronoid process when reconstruction of the radial head is not feasible, as described by Bellato et al. (reprinted from Bellato et al. [41] © 2016, with permission from Elsevier). **a** The medial side of the radial head over projecting the coronoid process of the proximal ulna. **b** Lateral view, the medial side of the radial head used as an autograft for the fractured coronoid process, left elbow. **c** Anterior view, the medial side of the radial head used as an autograft for the fractured coronoid process, left elbow, *M* medial, *L* lateral

microarchitecture and related these to clinically observed fracture patterns within the radial head.

Subdividing the radial head in VOIs to study the trabecular bone microarchitecture is not yet common in clinical studies, likely because of the limited spatial resolution of typical clinical in vivo imaging systems (200–500 µm or worse) to accurately visualize and hence quantify the trabecular structures [24, 36]. We used micro-CT at 17 µm pixel size, basing our approach on previous micro-CT imaging studies of the radial head [7] and performed the subdivision in quadrants according to clinical fracture mapping of the radial head [5]. Moreover, high-resolution peripheral quantitative CT (HR-pQCT) systems with a pixel size of up to 82 (and more recently of 61) µm have become available on the market, for scanning peripheral parts of the human body in vivo, such as the wrist and ankle [36, 37]. Those preclinical systems enable examination of the bone microarchitecture directly in patients in vivo, with a spatial resolution that approximates that of micro-CT. It can be expected that also those HR-pQCT systems will be increasingly used in research in future, including the proximal radius.

In case of comminuted radial head fractures with less than 3 fragments, open reduction and internal fixation (ORIF) using headless low-profile or conventional screws could be indicated [38, 39]. In daily practice, it is aimed to position the screws perpendicular to the fracture line of the radial head fracture, whereas crossed screws are used in case of radial neck fractures [40]. This study demonstrates that the best bone stock is present in the medial side of the radial head. Therefore, we suggest, if the fracture pattern of the radial head allows for this, to involve the medial side of the radial head in the positioning of the screws. In case of a terrible triad injury, where reconstruction of both the comminuted radial head- and coronoid fracture is not feasible, the discarded radial head could be used as an osteochondral graft (Fig. 7) [41, 42]. Based on our results, we suggest using the medial side of the radial head, since this part has more bone stock, possibly enabling a stronger fixation.

In conclusion, bone microstructural investigation of the proximal radius reveals groups of trabecular struts spanning from the foveal joint surface towards the medial and lateral cortices, distributing everyday joint loads. Our results indicate that the lateral side of the radial head contains lower bone volume fraction, trabecular number and higher separation compared to the medial side. This suggests that the lateral side is the mechanically weaker region of the radial head, particularly so in case of an impact load through the joint. The underlying bone microstructure in combination with the nature of the trauma mechanism during a fall, in which the forearm is frequently pronated, could explain the genesis of possible fracture patterns of the radial head, in particular more often involving the anterolateral quadrant. In addition, if screw fixation in radial head fractures is considered, surgeons should take advantage of the of the greater bone volume fraction in the medial side of the radial head, should the fracture line allow this.

Acknowledgements We thank the Ray Last Anatomy Laboratory at The University of Adelaide for the provision of cadaveric bone specimens, Adelaide Microscopy for providing access to the micro-CT system, Dr. Marco Palanca for valuable suggestions, The International Society of Arthroscopy, Knee Surgery and Orthopaedic Sports Medicine (ISAKOS) for covering the costs of micro-CT imaging.

Funding This study was funded by the International Society of Arthroscopy, Knee Surgery and Orthopaedic Sports Medicine (ISAKOS) to cover the costs of micro-CT imaging.

Compliance with ethical standards

Conflict of Interest Author #1 received an unrestricted Research Grant from the Marti-Keuning-Eckhardt Foundation, Jo Kolk Foundation and Michael-van Vloten Foundation. Author #4 received an unrestricted Postdoc Research Grant from the Marti-Keuning-Eckhardt Foundation. Other authors declare that they have no conflict of interest.

References

1. Bryce CD, Armstrong AD (2008) Anatomy and biomechanics of the elbow. Orthop Clin North Am 39(2):141–154. https://doi.org/10.1016/j.ocl.2007.12.001
2. Captier G, Canovas F, Mercier N, Thomas E, Bonnel F (2002) Biometry of the radial head: biomechanical implications in pronation and supination. Surg Radiol Anat 24(5):295–301. https://doi.org/10.1007/s00276-002-0059-9
3. Cone RO, Szabo R, Resnick D, Gelberman R, Taleisnik J, Gilula LA (1983) Computed tomography of the normal radioulnar joints. Invest Radiol 18(6):541–545
4. Haverstock JP, Katchky RN, Lalone EA, Faber KJ, King GJ, Athwal GS (2012) Regional variations in radial head bone volume and density: implications for fracture patterns and fixation. J Shoulder Elbow Surg 21(12):1669–1673. https://doi.org/10.1016/j.jse.2012.07.002
5. Mellema JJ, Eygendaal D, van Dijk CN, Ring D, Doornberg JN (2016) Fracture mapping of displaced partial articular fractures of the radial head. J Shoulder Elbow Surg 25(9):1509–1516. https://doi.org/10.1016/j.jse.2016.01.030
6. Yeung C, Deluce S, Willing R, Johnson M, King GJ, Athwal GS (2015) Regional variations in cartilage thickness of the radial head: implications for prosthesis design. J Hand Surg Am 40(12):2364–2371. https://doi.org/10.1016/j.jhsa.2015.09.005 (**(e2361)**)
7. Adikrishna A, Shin YH, Zulkarnain RF, Hong H, Sun Y, Jeon IH (2017) Beveled posteromedial corner of the radial head: a three-dimensional micro-computed tomography modeling study. J Anat 231(5):690–697. https://doi.org/10.1111/joa.12672
8. Gebauer M, Barvencik F, Mumme M, Beil FT, Vettorazzi E, Rueger JM, Pueschel K, Amling M (2010) Microarchitecture of the radial head and its changes in aging. Calcif Tissue Int 86(1):14–22. https://doi.org/10.1007/s00223-009-9304-0
9. Low SC, Bain GI, Findlay DM, Eng K, Perilli E (2014) External and internal bone micro-architecture in normal and Kienböck's lunates: a whole-bone micro-computed tomography study. J Orthop Res 32(6):826–833
10. Perilli E, Bala Y, Zebaze R, Reynolds KJ, Seeman E (2015) regional heterogeneity in the configuration of the intracortical canals of the femoral shaft. Calcif Tissue Int 97(4):327–335. https://doi.org/10.1007/s00223-015-0014-5
11. Perilli E, Baruffaldi F, Visentin M, Bordini B, Traina F, Cappello A, Viceconti M (2007) MicroCT examination of human bone specimens: effects of polymethylmethacrylate embedding on structural parameters. J Microsc 225(Pt 2):192–200. https://doi.org/10.1111/j.1365-2818.2007.01731.x
12. Perilli E, Briggs AM, Kantor S, Codrington J, Wark JD, Parkinson IH, Fazzalari NL (2012) Failure strength of human vertebrae: prediction using bone mineral density measured by DXA and bone volume by micro-CT. Bone 50(6):1416–1425. https://doi.org/10.1016/j.bone.2012.03.002
13. Roberts BC, Thewlis D, Solomon LB, Mercer G, Reynolds KJ, Perilli E (2017) Systematic mapping of the subchondral bone 3D microarchitecture in the human tibial plateau: variations with joint alignment. J Orthop Res 35(9):1927–1941
14. Zumstein MA, Raniga S, Labrinidis A, Eng K, Bain GI, Moor BK (2016) Optimal lateral row anchor positioning in posterior-superior transosseous equivalent rotator cuff repair: a micro-computed tomography study. Orthop J Sports Med 4(11):2325967116671305
15. Martelli S, Perilli E (2018) Time-elapsed synchrotron-light microstructural imaging of femoral neck fracture. J Mech Behav Biomed Mater 84:265–272. https://doi.org/10.1016/j.jmbbm.2018.05.016
16. Duckworth AD, Clement ND, Jenkins PJ, Aitken SA, Court-Brown CM, McQueen MM (2012) The epidemiology of radial head and neck fractures. J Hand Surg Am 37(1):112–119. https://doi.org/10.1016/j.jhsa.2011.09.034
17. Beingessner DM, Dunning CE, Gordon KD, Johnson JA, King GJ (2004) The effect of radial head excision and arthroplasty on elbow kinematics and stability. J Bone Joint Surg Am 86-A(8):1730–1739
18. Morrey BF, Tanaka S, An KN (1991) Valgus stability of the elbow. A definition of primary and secondary constraints. Clin Orthop Relat Res 265:187–195
19. Smith GR, Hotchkiss RN (1996) Radial head and neck fractures: anatomic guidelines for proper placement of internal fixation. J Shoulder Elbow Surg 5(2 Pt 1):113–117
20. van Leeuwen DH, Guitton TG, Lambers K, Ring D (2012) Quantitative measurement of radial head fracture location. J Shoulder Elbow Surg 21(8):1013–1017. https://doi.org/10.1016/j.jse.2011.08.056
21. Amis AA, Miller JH (1995) The mechanisms of elbow fractures: an investigation using impact tests in vitro. Injury 26(3):163–168
22. Koslowsky TC, Mader K, Brandenburg A, Hellmich M, Koebke J (2008) Subchondral bone density of the radial head measured with subtraction densitometry. Surg Radiol Anat 30(2):113–118. https://doi.org/10.1007/s00276-007-0299-9
23. Tassani S, Perilli E (2013) On local micro-architecture analysis of trabecular bone in three dimensions. Int Orthop 37(8):1645–1646. https://doi.org/10.1007/s00264-013-1989-z
24. Perilli E, Parkinson IH, Reynolds KJ (2012) Micro-CT examination of human bone: from biopsies towards the entire organ. Annali dell'Istituto superiore di sanità 48(1):75–82
25. Parfitt AM, Drezner MK, Glorieux FH, Kanis JA, Malluche H, Meunier PJ, Ott SM, Recker RR (1987) Bone histomorphometry: standardization of nomenclature, symbols, and units. Report of the ASBMR histomorphometry nomenclature committee. J Bone Miner Res 2(6):595–610. https://doi.org/10.1002/jbmr.5650020617
26. Perilli E, Baruffaldi F, Bisi MC, Cristofolini L, Cappello A (2006) A physical phantom for the calibration of three-dimensional X-ray microtomography examination. J Microsc 222(Pt 2):124–134. https://doi.org/10.1111/j.1365-2818.2006.01580.x
27. Hildebrand T, Ruegsegger P (1997) Quantification of bone microarchitecture with the structure model index. Comput Method Biomech Biomed Engin 1(1):15–23. https://doi.org/10.1080/01495739708936692
28. Ruff C, Holt B, Trinkaus E (2006) Who's afraid of the big bad Wolff?:"Wolff's law" and bone functional adaptation. Am J Phys Anthropol 129(4):484–498
29. Sardelli M, Tashjian RZ, MacWilliams BA (2011) Functional elbow range of motion for contemporary tasks. J Bone Joint Surg Am 93(5):471–477. https://doi.org/10.2106/JBJS.I.01633

30. Morrey BF, An KN, Stormont TJ (1988) Force transmission through the radial head. J Bone Joint Surg Am 70(2):250–256
31. van Riet RP, Van Glabbeek F, Baumfeld JA, Neale PG, Morrey BF, O'Driscoll SW, An KN (2006) The effect of the orientation of the radial head on the kinematics of the ulnohumeral joint and force transmission through the radiocapitellar joint. Clin Biomech (Bristol, Avon) 21(6):554–559. https://doi.org/10.1016/j.clinbiomech.2006.01.006
32. Kaas L, Sierevelt IN, Vroemen JP, van Dijk CN, Eygendaal D (2012) Osteoporosis and radial head fractures in female patients: a case-control study. J Shoulder Elbow Surg 21(11):1555–1558. https://doi.org/10.1016/j.jse.2012.03.007
33. Kaas L, van Riet RP, Vroemen JP, Eygendaal D (2010) The epidemiology of radial head fractures. J Shoulder Elbow Surg 19(4):520–523. https://doi.org/10.1016/j.jse.2009.10.015
34. Perilli E, Baleani M, Öhman C, Fognani R, Baruffaldi F, Viceconti M (2008) Dependence of mechanical compressive strength on local variations in microarchitecture in cancellous bone of proximal human femur. J Biomech 41(2):438–446. https://doi.org/10.1016/j.jbiomech.2007.08.003
35. Seeman E (2013) Age- and menopause-related bone loss compromise cortical and trabecular microstructure. J Gerontol A Biol Sci Med Sci 68(10):1218–1225. https://doi.org/10.1093/gerona/glt071
36. Nishiyama KK, Shane E (2013) Clinical imaging of bone microarchitecture with HR-pQCT. Curr Osteoporos Rep 11(2):147–155. https://doi.org/10.1007/s11914-013-0142-7
37. Kroker A, Zhu Y, Manske SL, Barber R, Mohtadi N, Boyd SK (2017) Quantitative in vivo assessment of bone microarchitecture in the human knee using HR-pQCT. Bone 97:43–48. https://doi.org/10.1016/j.bone.2016.12.015
38. Ring D, Quintero J, Jupiter JB (2002) Open reduction and internal fixation of fractures of the radial head. J Bone Joint Surg Am 84-A(10):1811–1815
39. Adams JE, Sems SA, Steinmann SP (2017) Open treatment of radial head fractures. JBJS Essent Surg Tech 7(4):e35. https://doi.org/10.2106/JBJS.ST.15.00073
40. Duckworth AD, McQueen MM, Ring D (2013) Fractures of the radial head. Bone Joint J 95-B(2):151–159. https://doi.org/10.1302/0301-620X.95B2.29877
41. Bellato E, Rotini R, Marinelli A, Guerra E, O'Driscoll SW (2016) Coronoid reconstruction with an osteochondral radial head graft. J Shoulder Elbow Surg 25(12):2071–2077. https://doi.org/10.1016/j.jse.2016.09.003
42. Ring D, Guss D, Jupiter JB (2012) Reconstruction of the coronoid process using a fragment of discarded radial head. J Hand Surg Am 37(3):570–574. https://doi.org/10.1016/j.jhsa.2011.12.016